Application of [Co(Corrole)]- Complexes in Ring-Closing C-H Amination of Aliphatic Azides via Nitrene Radical Intermediates

Goswami, M.; Geuijen, P.; Reek, J.N.H.; de Bruin, B.

DOI
10.1002/ejic.201701343

Publication date
2018

Document Version
Final published version

Published in
European Journal of Inorganic Chemistry

ChemPubSoc Europe

DOI: 10.1002/ejic.201701343

EurJIC European Journal of Inorganic Chemistry

Full Paper

Cobalt Corrole Activation of Azides

Application of [Co(Corrole)]$^-$ Complexes in Ring-Closing C–H Amination of Aliphatic Azides via Nitrene Radical Intermediates

Monalisa Goswami,[a] Paul Geuijen,[a] Joost. N. H. Reek,[a] and Bas de Bruin*[a]

Abstract: The synthesis, characterisation and application of anionic [Co^{II}(Cor)]$^-$ (Cor = corrole) metalloradicals in the ring-closing C–H amination of an aliphatic azide in the presence of Boc_2O (Boc = *tert*-butyloxycarbonyl) to give the corresponding Boc-protected N-heterocyclic product *tert*-butyl 2-phenylpyrrolidine-1-carboxylate are reported. This is the first example of the use of metalloradical cobalt(II) corrole complexes in nitrene-transfer reactions. On the basis of DFT calculations, the reaction is proposed to proceed via discrete open-shell nitrene radical intermediates bearing most of their spin density at the nitrene nitrogen atom. The [Co^{II}(Cor)]$^-$ complexes are substantially faster catalysts than the corresponding neutral [Co^{II}(porphyrin)] complexes when applied in the same ring-closing C–H amination reaction under identical reaction conditions. Increasing the electron density at cobalt(II) therefore has a positive influence on the reaction rate.

Introduction

Nitrogen-containing ring compounds are among the most commonly found heterocycles in natural products and pharmaceuticals.[1] Synthesising such heterocycles by direct C–H amination, that is, C–H activation combined with a C–N bond-forming ring-closing step, is time- and atom-efficient and hence an attractive way to make such compounds. One strategy to achieve this goal is via reactive metallo-nitrene intermediates.[2] In this method a metal catalyst activates a nitrene precursor to form a metallo-nitrene intermediate. Depending on its reactivity, this metallo-nitrene intermediate can insert into challenging bonds, such as thermodynamically and kinetically stable C–H bonds.[3] Organic azides are particularly attractive nitrene precursors in this regard, as they are easy to synthesise and generate only N_2 as a waste product in the amination step.[3,4] However, only a handful of examples in which organic azides are used in intramolecular C–H amination reactions to form N-heterocyclic compounds have been reported.[5,6] Particular systems of relevance to the results described in this paper that have proven to be successful in C–H bond amination are cobalt(II) porphyrin (Por) catalysts (Scheme 1). These [Co^{II}(Por)] catalysts are in general capable of a variety of nitrene-transfer reactions from azides. In addition to the inter- and intramolecular aziridination reactions,[7] also a variety of intermolecular[8] and intramolecular[9] benzylic/allylic/benzallylic C–H amination reactions have been reported. Typically, activated azides are used as the substrates in these reactions, such as carbamoyl, sulfonyl or phosphoryl azides.[10] DFT mechanistic studies revealed a stepwise mechanism involving an experimentally well characterised Co^{III} nitrene radical intermediate.[11] DFT calculations further suggested that the rate-determining step of these catalytic reactions is the activation of the azide at the metal centre,[12] which has a substantial barrier. Consequently, in many of these transformations high reaction temperatures are required.[7–13] This is most evident in reactions involving unactivated alkyl azides (azide moiety positioned directly next to a CH_2 group), which require heating to at least around 100 °C to activate the azide with [Co^{II}(Por)] catalysts.[13] The generalised mechanism proposed for these reactions involves rate-limiting azide activation followed by hydrogen-atom transfer from a benzylic C–H bond to the thus-formed nitrene radical. A subsequent radical rebound step, followed by dissociation and trapping of the cyclic amine by Boc_2O (Boc = *tert*-butyloxycarbonyl) to produce the Boc-protected product, completes the catalytic cycle

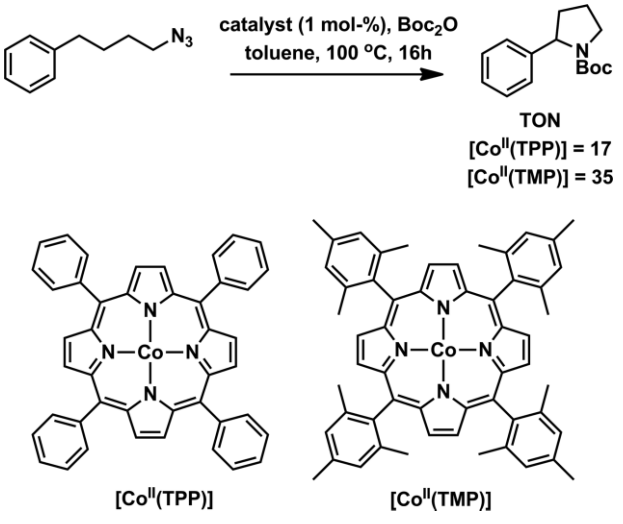

Scheme 1. [Co^{II}(Por)]-catalysed intramolecular C–H amination of aliphatic azides mediated by [Co(Por)] complexes.

[a] *Van 't Hoff Institute for Molecular Sciences, University of Amsterdam, Science Park 904, 1098 XH Amsterdam, The Netherlands*
E-mail: b.debruin@uva.nl
http://homkat.nl

Supporting information and ORCID(s) from the author(s) for this article are available on the WWW under https://doi.org/10.1002/ejic.201701343.

(Scheme 2).[13] Notably, in the azide-activation step the metal centre is oxidised from cobalt(II) to cobalt(III) to generate the required nitrene radical intermediate. Hence, we expected that application of ligands imposing a higher electron density at the cobalt centre could be beneficial in leading to faster catalytic reactions by lowering the barrier of the rate-limiting N_2-dissociation step. Some earlier studies seem to confirm this hypothesis in an indirect manner,[6] but the beneficial effect of electron-donating ligands on the rate of these reactions is evident from recent studies performed by us.[13] In a direct comparative study, the electron-rich [Co^{II}(TMP)] was shown to outperform [Co^{II}(TPP)] in the intramolecular C–H amination of aliphatic azides (Scheme 1).

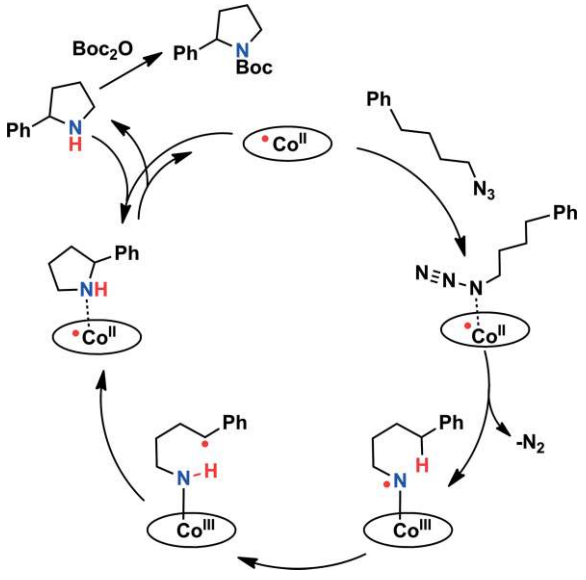

Scheme 2. Generalized mechanism for catalytic ring-closing C–H amination of an aliphatic azide catalysed by planar low-spin Co^{II} complexes.

We hypothesised that a ligand scaffold that retains the square-planar geometry of a porphyrin but is more electron-rich could well be beneficial for the activation of aliphatic azides. Hence, we turned our attention to the corrole macrocycle. Corroles are tetrapyrrolic compounds related to porphyrins. The difference to porphyrins is that in corroles one of the methine bridges that link the pyrrole units together has been replaced with a direct pyrrole–pyrrole bond (Figure 1). Thus, corroles have a trianionic charge when bound to transition metals, and there is one position less to attach the *meso* substituents. As a consequence, corroles have a slightly smaller metal-binding pocket allowing for a "tighter grip" on the metal centre. In addition, there is one less carbon atom in the aromatic ring of corroles, which, besides the trianionic charge of a corrole ligand, substantially increases the electron density of the metal centre in corrole complexes compared to the corresponding porphyrin complexes. As a result, corroles are expected to stabilize transition metals in higher oxidation states, even better so than porphyrins. This feature is expected to have a positive influence on the azide-activation step at the metal centre of the catalyst, in which cobalt(II) undergoes one-electron oxidation. Previously, corrole complexes of cobalt have been extensively studied,[14] amongst others for water oxidation and oxygen reduction reactions. However, monoanionic cobalt(II) corrole complexes have so far never been employed as metalloradical catalysts for nitrene or carbene insertion into C–H bonds. This provides an opportunity to study the metalloradical reactivity of monoanionic [Co^{II}(Cor)]$^-$ complexes in mediating catalytic radical-type reactions in general, and in particular for the nitrene-radical ring-closing C–H amination reactions described herein.

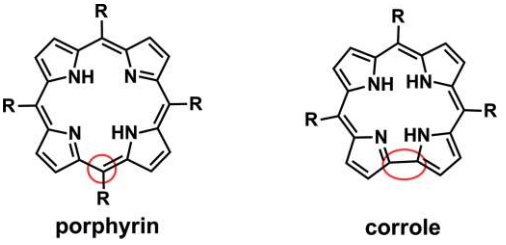

Figure 1. Related tetradentate macrocycles used in cobalt(II)-mediated C–H bond amination reactions: porphyrins (left) and corroles (right).

Results and Discussion

To test the feasibility of corroles as ligands in cobalt(II)-catalysed nitrene-transfer reactions, we synthesised three corrole ligands with electronically different substituents (Figure 2).

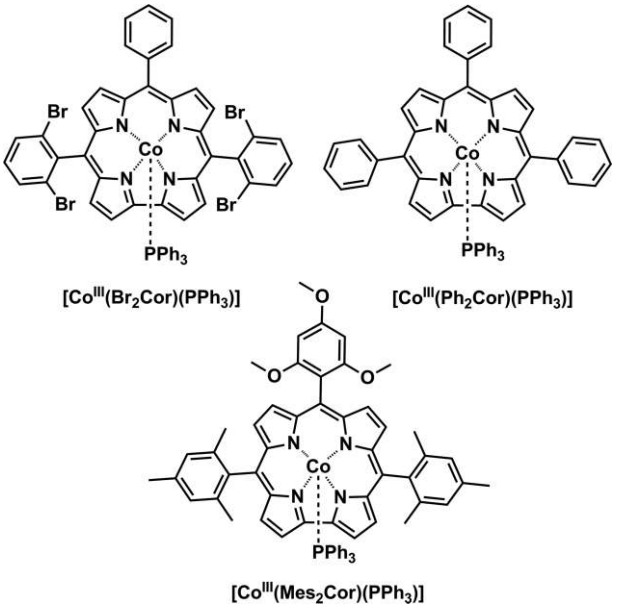

Figure 2. Three [Co^{III}(Cor)] complexes with varying substituents applied in the ring-closing C–H amination of alkyl azides.

In their monoreduced (monoanionic) cobalt(II) forms, all of these complexes should have substantially higher electron density at the metal centre than the corresponding cobalt(II) porphyrin complexes.[15] Additionally, the electronic properties in the series of corrole complexes differ. Dibromo-substituted [Co^{III}(Br_2Cor)(PPh_3)] should contain the least electron rich corrole, mesityl-substituted [Co^{III}(Mes_2Cor)(PPh_3)] should contain the most electron-rich corrole, and the (unsubstituted) [Co^{III}(Ph_2Cor)(PPh_3)] should have electronic properties in-

between those of [$Co^{III}(Br_2Cor)(PPh_3)$] and [$Co^{III}(Mes_2Cor)(PPh_3)$]. Reduction of these complexes with a suitable chemical reductant should produce the corresponding monoanionic metalloradical [$Co^{II}(Cor)]^-$ complexes. To find the right reducing agent for reduction of cobalt(III) to cobalt(II), we first studied the electrochemical properties of the [$Co^{III}(Cor)(PPh_3)$] complexes. The three corroles were synthesised via the dipyrromethane route, following the procedures reported by Gryko and co-workers with some minor modifications (Scheme 3).[16] Details of the synthetic procedures are described in the Experimental Section.

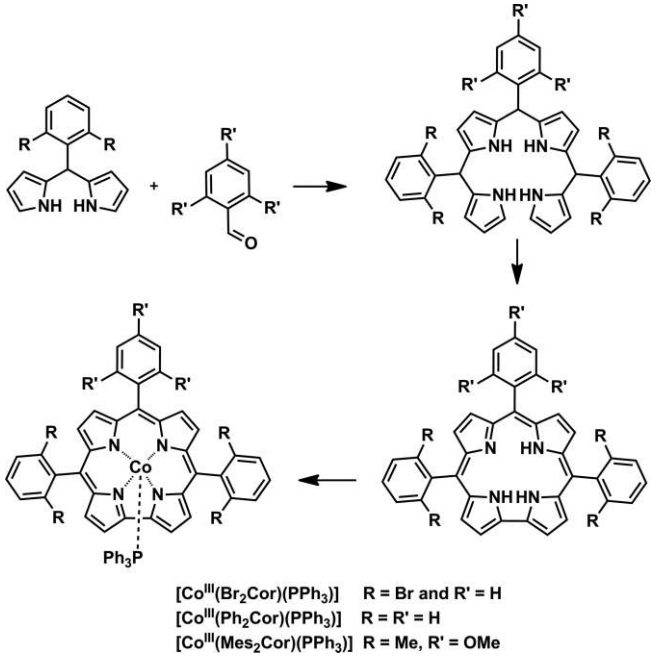

Scheme 3. Generalised scheme for the synthesis of the corrole complexes [$Co^{III}(Br_2Cor)(PPh_3)$], [$Co^{III}(Ph_2Cor)(PPh_3)$] and [$Co^{III}(Mes_2Cor)(PPh_3)$].

While the crystal structure of [$Co^{III}(Ph_2Cor)(PPh_3)$] has been reported, the X-ray structural data of [$Co^{III}(Br_2Cor)(PPh_3)$] and [$Co^{III}(Mes_2Cor)(PPh_3)$] were previously unknown. We were able to grow crystals of these complexes. The molecular structure of [$Co^{III}(Br_2Cor)(PPh_3)$] and some relevant bond lengths are shown in Figure 3. The Co–N(corrole) bonds are significantly shorter than Co–N(porphyrin) bonds {1.867 and 1.880 in [$Co^{III}(Br_2Cor)(PPh_3)$] vs. 1.949 in [$Co^{II}(TPP)$]}.[17] This is expected, because of the trianionic charge and the smaller ring size of the corrole macrocycle.

For [$Co^{III}(Mes_2Cor)(PPh_3)$] the atom connectivity could be satisfactorily determined and confirmed the structure of the complex. However, the X-ray data of [$Co^{III}(Mes_2Cor)(PPh_3)$] were of insufficient quality to derive any reliable information about the bond lengths. This structure is shown in the Experimental Section (Figure 9).

Cyclic voltammetry (CV) was used to study the redox behaviour of the three above-mentioned [$Co^{III}(Cor)(PPh_3)$] complexes.[18,19] For the application of these complexes as catalysts in nitrene-transfer reactions, we were particularly interested in

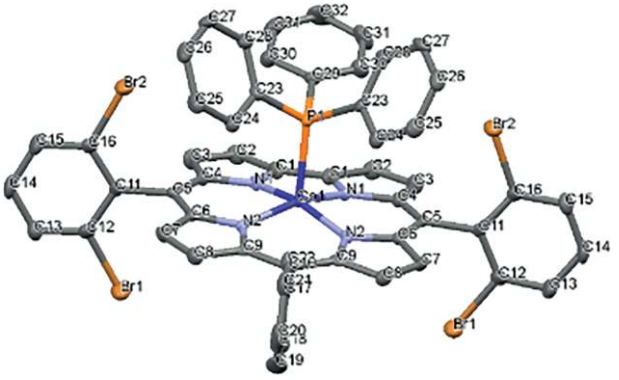

Figure 3. Displacement-ellipsoid plot of [$Co^{III}(Br_2Cor)(PPh_3)$]. Hydrogen atoms are omitted for clarity. Selected bond lengths [Å]: Co–N1 1.867(5), Co–N2 1.880(5), Co–P1 2.225(3), Br1–C12 1.895(7), Br2–C16 1.891(6), N1–C 11.354(8), N1–C4 1.380(7), N2–C9 1.386 (8) N2–C6 1.400(7), C11–C51.516(8).

the first reduction waves and the corresponding re-oxidation waves of these complexes. The first (chemically irreversible) reduction peak potential is important for choosing a suitable chemical reductant that reduces the parent [$Co^{III}(Cor)(PPh_3)$] complexes to corresponding monoanionic [$Co^{III}(Cor)(PPh_3)]^-$ complexes without over-reduction. The corresponding re-oxidation peak potential gives direct information about the reductive power of the corresponding monoanionic [$Co^{II}(Cor)]^-$ complexes after PPh_3 dissociation.[20]

The [$Co^{III}(Cor)(PPh_3)$] complexes show the expected redox behaviour, similar to that observed previously for related complexes.[20] The first one-electron reduction process is electrochemically irreversible for all these complexes, at least at the applied scan rate of 100 mV s^{-1} of the CV measurements (Figure 4A–C). The first reduction wave is coupled to an anodically shifted re-oxidation wave for all complexes, in an overall chemically reversible electrochemical–chemical–electrochemical–chemical (ECEC) process (Figure 4D). A second reduction peak at more negative potentials is also observed for all these complexes, which is fully reversible in all cases (see Figure S1). In accordance with the electronic nature of the substituents, the peak potential of the first reduction process shifts to more negative potentials upon increasing the electron-donating properties of the substituents (Table 1): [$Co^{III}(Mes_2Cor)(PPh_3)$] < [$Co^{III}(Ph_2Cor)(PPh_3)$] < [$Co^{III}(Br_2Cor)(PPh_3)$]. On the basis of these peak potentials, cobaltocene ($CoCp_2$; $E_{1/2} \approx -1.3$ V vs. $Fc^{0/+}$) or decamethylcobaltocene ($CoCp^*_2$; $E_{1/2} \approx -1.9$ V vs. $Fc^{0/+}$) can be used as a suitable reductant for these complexes.[21] The ECEC sequence of events explaining the observed behaviour of the first reduction process with an anodically shifted re-oxidation wave is schematically shown in Figure 4D. One-electron reduction of the parent [$Co^{III}(Cor)(PPh_3)$] complex at the metal centre leads to the formation of an anionic [$Co^{II}(Cor)(PPh_3)]^-$ complex, followed by PPh_3 dissociation producing [$Co^{II}(Cor)]^-$. Oxidation of [$Co^{II}(Cor)]^-$ to [$Co^{III}(Cor)$] occurs at a higher redox potential than reduction of [$Co^{III}(Cor)(PPh_3)$] to [$Co^{II}(Cor)(PPh_3)]^-$, and is followed by re-coordination of PPh_3 to regenerate the parent [$Co^{III}(Cor)(PPh_3)$] complex.[20]

EPR spectroscopic and UV/Vis spectro-electrochemical (SEC) measurements were performed to confirm the ECEC mecha-

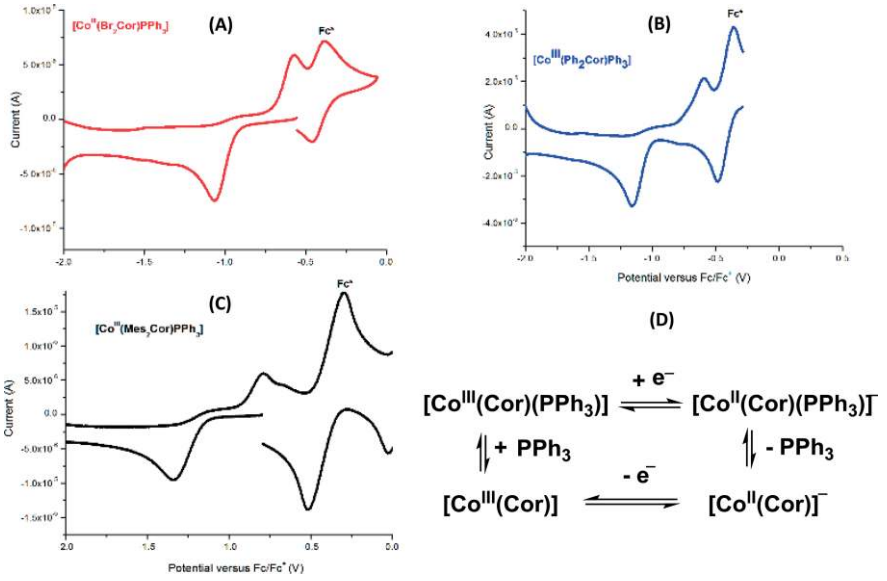

Figure 4. (A) CV of $[Co^{III}(Br_2Cor)(PPh_3)]$, (B) CV of $[Co^{III}(Ph_2Cor)(PPh_3)]$, (C) CV of $[Co^{III}(Mes_2Cor)(PPh_3)]$ in THF referenced against $Fc^{0/+}$ [with bis(pentamethylcyclopentadienyl)iron (Fc*) as internal standard]. (D) Schematic representation of different species present during the reduction and re-oxidation events during the CV scan.

Table 1. Peak currents for the first reduction and the corresponding re-oxidation wave of the three complexes referenced against the $Fc^{0/+}$ couple, measured in THF by using Fc* as internal standard (colour codes follow those of Figure 4).

Complex	E_{red}^{peak} [V]	E_{ox}^{peak} [V]
$[Co^{III}(Br_2Cor)(PPh_3)]$	–1.06	–0.56
$[Co^{III}(Ph_2Cor)(PPh_3)]$	–1.15	–0.59
$[Co^{III}(Mes_2Cor)(PPh_3)]$	–1.34	–0.79

nism shown in Figure 4D. The SEC measurements were performed by coupling coulometric CV experiments to UV/Vis measurements in an optically transparent thin-layer electrochemical (OTTLE) cell. These experiments also allowed us to determine whether any decomposition occurs on the coulometric timescale or any long-lived intermediates are formed during the reduction/re-oxidation events. Upon one-electron reduction, in all cases the absorbance of the Soret bands undergoes a bathochromic shift with the absorbance around 380 nm decreasing in intensity and a new absorbance arising around 420 nm. In addition, the absorbance of the Q bands between 550 and 700 nm shows an increase in intensity, probably due to a decreased difference in energy between the π–π* orbitals of the reduced complex. The rather small red shifts observed are strongly suggestive of PPh_3 dissociation upon reduction. A representative example of the spectral changes observed upon reduction of $[Co^{III}(Ph_2Cor)(PPh_3)]$ is shown in Figure 5. For similar spectra of the two other complexes, see Figure S2. When the complexes are re-oxidised (at the anodically shifted redox potential), the original $[Co^{III}(Ph_2Cor)(PPh_3)]$ complex is cleanly regenerated from the $[Co^{II}(Ph_2Cor)]^-$ complex, as evidenced by the UV/Vis measurements. Multiple isosbestic points are indicative of clean interconversion of the reduced and oxidized species without long-lived intermediates.

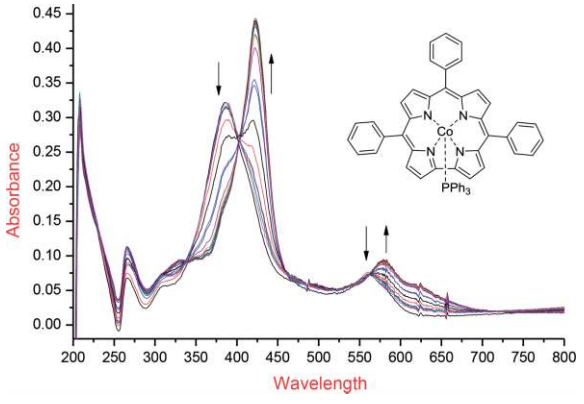

Figure 5. UV/Vis spectra obtained in the spectro-electrochemical experiments on $[Co^{III}(Ph_2Cor)(PPh_3)]$.

Having determined the reduction peak potentials of these complexes and their clean conversion to the reduced species, we performed X-band EPR studies. Using a chemical reductant ($CoCp_2$ for $[Co^{III}(Br_2Cor)(PPh_3)]$ and $[Co^{III}(Ph_2Cor)(PPh_3)]$ and $CoCp^*_2$ for $[Co^{III}(Mes_2Cor)(PPh_3)]$), all of these complexes could be reduced to give species with EPR spectra [anisotropic spectra, measured at 20 K in a 2-methyltetrahydrofuran (MeTHF) glass] characteristic for formation of cobalt(II) metalloradicals. The EPR spectrum of $[Co^{II}(Mes_2Cor)]^-$ is shown in Figure 6.[22] For EPR spectra of the other complexes, see Figure S3. The EPR spectrum shown in Figure 6 reveals clear cobalt hyperfine couplings along the two higher g values ($g_{11} = 3.56$, $A_{11}^{Co} = 740$ MHz; $g_{22} = 2.22$, $A_{22}^{Co} = 260$ MHz) and a sharper, almost featureless line at the lowest g value ($g_{33} = 1.85$). No (resolved) phosphorus hyperfine couplings are visible along any of these directions in the anisotropic spectrum, in agreement with PPh_3 dissociation upon one-electron reduction of $[Co^{III}(Mes_2Cor)(PPh_3)]$.[23]

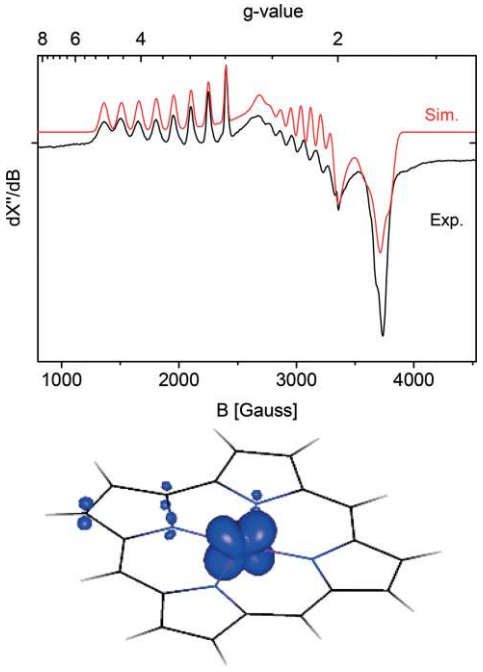

Figure 6. Top: Experimental and simulated EPR spectra of the $[Co^{III}(Mes_2Cor)]^-$ complex formed upon reduction of $[Co^{III}(Mes_2Cor)(PPh_3)]$ with $CoCp^*_2$, measured at 20 K in a MeTHF glass. Microwave frequency = 9.38412 GHz, modulation amplitude = 0.1 G, power = 2 mW. Bottom: DFT calculated spin-density distribution of the $[Co^{III}(Cor)]^-$ complex showing that the unpaired electron resides in a d_{xy} orbital.

DFT optimisation of the anionic $[Co^{II}(Cor)]^-$ complex clearly showed that the SOMO is the d_{xy} orbital (Figure 6, bottom), and this leads to different spin–orbit interactions than in related $[Co^{II}(Por)]$ complexes. This is in agreement with the EPR spectra of the corrole being distinctly different from those of the related porphyrin complexes.[24]

We tested the activity and selectivity of the three monoanionic $[Co^{II}(Cor)]^-$ complexes in the direct ring-closing reaction of (4-azidobutyl)benzene to give the N-heterocyclic pyrrolidine product. This reaction was reported to proceed with $[Co^{II}(TMP)]$ to selectively produce the Boc-protected pyrrolidine product *tert*-butyl 2-phenylpyrrolidine-1-carboxylate.[13] The high barrier and slow reactions associated with the Co(Por)-catalysed process prompted us to test the more electron rich monoanionic cobalt(II) corrole complexes as catalysts for this reaction. We argued that more facile electron transfer from cobalt(II) to the nitrene moiety generated at cobalt upon N_2 loss from the coordinated aliphatic azide in the transition state for nitrene-radical formation might lead to a lower barrier of the rate-limiting azide-activation step. Thus, using the same reaction conditions as reported for the $[Co^{II}(TMP)]$ system, we performed this reaction with the $[Co^{II}(Cor)]^-$ complexes described above. These were generated from the corresponding $[Co^{III}(Cor)(PPh_3)]$ complexes by one-electron reduction with a suitable cobaltocene reducing agent prior to catalysis. We monitored the appearance of the product and disappearance of the azide substrate with

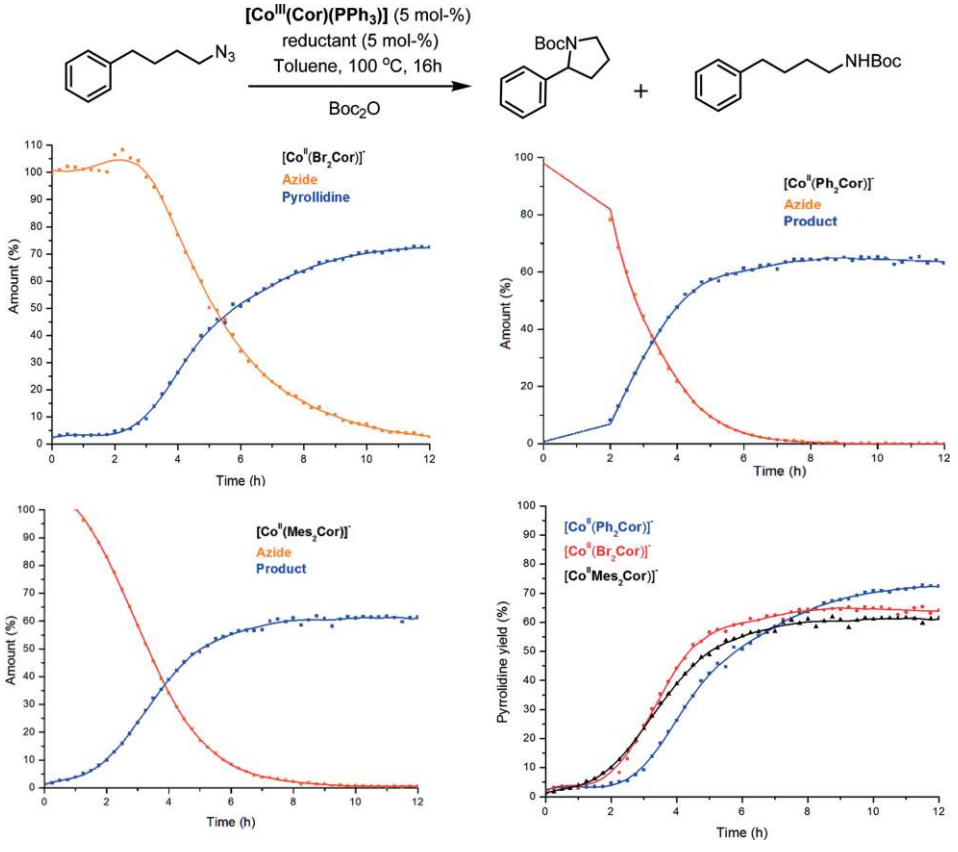

Figure 7. Reaction profiles for the ring-closing C–H amination. Top left: $[Co^{II}(Br_2Cor)]^-$, top right: $[Co^{II}(Ph_2Cor)]^-$ and bottom left: $[Co^{II}(Mes_2Cor)]^-$. Bottom right: overlay of the pyrrolidine product formation {red: $[Co^{II}(Br_2Cor)]^-$; blue: $[Co^{II}(Ph_2Cor)]^-$; black: $[Co^{II}(Mes_2Cor)]^-$}.

Table 2. Performance of different $[Co^{II}(Cor)]^-$ catalysts in the intramolecular ring-closing C–H amination of (4-azidobutyl)benzene to give the corresponding Boc-protected pyrrolidine.[a]

Entry	Catalyst	Solvent	Remarks	Pyrrolidine[b]	Linear product
1	$[Co^{II}(Br_2Cor)]^-$	toluene		73 %	–
2	$[Co^{II}(Ph_2Cor)]^-$	toluene		78 %	–
3	$[Co^{II}(Mes_2Cor)]^-$	toluene		64 %	–
4	any $[Co^{II}(Cor)]^-$	toluene	no Boc_2O	not observed	–
5	any $[Co^{II}(Cor)]^-$	toluene	no reductant	not observed	–
6	any $[Co^{II}(Cor)]^-$	THF		not observed	–
7	$[Co^{II}Ph_2(Cor)]^-$	acetonitrile/toluene		43 %	–
8	$[Co^{II}Ph_2(Cor)]^-$	CH_2Cl_2/toluene		31 %	15 %
9	$[Co^{II}Ph_2(Cor)]^-$	THF/toluene		11 %	–
10	$[Co^{II}Ph_2(Cor)]^-$	toluene	NBu_4PF_6 added	29 %	–
11	cobaltocene[c]	benzene		0 %	

[a] Reactions were performed on 0.3 mmol scale in dry toluene at 100 °C with 5 mol-% precatalyst, 5 mol-% reducing agent and 1.1 equiv. Boc_2O for 16 h. [b] ^1H NMR yields are reported with mesitylene as internal standard. [c] Data taken from ref.[6g]

time using NMR integrations against an internal standard (Figure 7).

In each case the azide substrate was fully consumed and pyrrolidine product was formed (Table 2, entries 1–3). In the absence of the reductant no reaction took place. This proves that it is only the reduced (Co^{II}) complex that is able to activate the azide in this reaction and not the parent Co^{III} complex itself (Table 2, entry 5).

Also, in the absence of Boc_2O no reaction took place. The same was observed in the cobalt-porphyrin-catalysed reactions, which was ascribed to product inhibition due to binding of the pyrrolidine product to cobalt(II) in absence of Boc_2O, while the Boc-protected pyrrolidine does not inhibit the reaction.[13] Product inhibition in absence of Boc_2O therefore also seems to be an issue in the cobalt(II)-corrole-catalysed reactions (Table 2, entry 4). For all three catalysts, the reaction has an initiation time of about 2 h before azide consumption starts (Figure 7). We ascribe this initiation time to the poor solubility of the $[Co^{II}(Cor)]^-$(cobaltocenium$^+$) salts in the low-polarity $[D_8]$toluene solvent used in these reactions. Upon reduction of the neutral $[Co^{III}(Cor)(PPh_3)]$ complexes to the anionic $[Co^{II}(Cor)]^-$ complexes, the solubility decreases drastically, which was also visually observable in the NMR tubes in which the reactions were monitored {near-quantitative precipitation of the $[Co^{II}(Cor)]^-$(cobaltocenium$^+$) salts is evident from a photograph of the NMR tube shown in Figure S5}. After heating to 100 °C for about 2 h in the presence of the azide, (part of) the complex is slowly solubilised, after which it can take part in the reaction. This process is most likely facilitated by a slow heterogeneous reaction between the azide and the precipitated $[Co^{II}(Cor)]^-$(cobaltocenium$^+$) salt. After the initiation lag time, the azide is fully consumed within about 6 h for all three corrole complexes investigated. This is a remarkable improvement in reaction rate (ca. 2.5-fold) compared to the benchmark $[Co^{II}(TMP)]$ system, which requires about 16 h before all the azide is consumed.[10] This proves that the more electron rich monoanionic $[Co^{II}(Cor)]^-$ complexes are indeed more active catalysts than the corresponding neutral porphyrin $[Co^{II}(Por)]$ complexes.

Notably, even though all azide substrate is consumed, the yield of the pyrrolidine product is not proportional to the consumption of the azide (based on ^1H NMR spectra). The highest yield of the pyrrolidine product (78 %) was obtained with the $[Co^{II}(Ph_2Cor)]^-$ catalyst. Hence, apart from the pyrrolidine product other, side products are produced as well. These are a mixture of several (uncharacterised) compounds that only give rise to small, poorly recognisable peaks in the ^1H NMR spectra of the crude reaction mixtures. So, while the activity of the system is increased, its selectivity is somewhat compromised. Formation of the linear *N*-Boc-protected amine product $Ph(CH_2)_4$-NHBoc provides only a partial explanation for the unaccounted mass balance. While $Ph(CH_2)_4NHBoc$ is a known by-product in related reactions,[6,10,13] it is only formed in minor amounts in the reactions studied here (see Table 2). A Staudinger reaction of PPh_3 liberated from the catalyst producing the iminophosphorane can account for at most 5 mol-% loss of the starting material. Hence, some other unidentified side products must be formed in these reactions.

As far as the relative performance of the three $[Co^{II}(Cor)]^-$ catalysts is concerned, $[Co^{II}(Ph_2Cor)]^-$ consistently gave the highest yields of the desired pyrrolidine product. The $[Co^{II}(Br_2Cor)]^-$ catalyst gave lower yields, and the lowest yields were obtained with the $[Co^{II}(Mes_2Cor)]^-$ catalyst. This behaviour is counterintuitive, as we expected best reaction results for the more electron rich $[Co^{II}(Mes_2Cor)]^-$ catalyst and the poorest for the least-electron rich $[Co^{II}(Br_2Cor)]^-$ catalyst. However, these yields do not correlate directly to the relative activities, as the rates {max. slopes in Figure 7, bottom right $[Co^{II}(Br_2Cor)]^-$ > $[Co^{II}(Ph_2Cor)]^-$ > $[Co^{II}(Mes_2Cor)]^-$} not only do not differ much, but these values are also likely to be influenced by the (slow and potentially different) rates of solubilisation of the salts. Furthermore, the $[Co^{II}(Mes_2Cor)]^-$ and $[Co^{II}(Br_2Cor)]^-$ catalysts are more sterically hindered around cobalt than the $[Co^{II}(Ph_2Cor)]^-$ catalyst. Thus, favourable electronic effects of electron-donating side groups at the corrole ring of these catalysts could well be (partly) counterbalanced by unfavourable steric interactions.

Next we tried to improve the efficiency of this reaction by attempting to increase the solubility of the in-situ-reduced catalyst. To determine whether the solubility of the reduced catalyst could be increased by changing the polarity of the reaction mixture, we tried a few other solvents (Table 2, entries 6–10). However, on changing to more polar solvents such as THF, no product formation was observed, and with solvent mixtures

such as acetonitrile/toluene, CH_2Cl_2/toluene and THF/toluene the yield of the pyrrolidine product dropped drastically. In the CH_2Cl_2/toluene mixture 15 % of the unwanted linear product was also observed. Also, with *N*-butylammonium phosphate as phase-transfer catalyst the yield of the pyrrolidine dropped to 29 % (Table 2, entry 10). Hence, it seems these reactions only work well in low-polarity aromatic solvents such as toluene and benzene, at least for the $[Co^{II}(Cor)]^-$ catalysts studied here.

DFT Calculations

Next, to confirm whether indeed the azide-activation step has a lower barrier for the anionic $[Co^{II}(Cor)]^-$ systems compared to the corresponding neutral $[Co^{II}(Por)]$ systems, we computed the free-energy barrier of this step using DFT methods. The calculations were performed at the BP86 and def2-TZVP level of theory for the non-functionalised $[Co^{II}(Cor)]^-$ system. The choice of this computational method is based on previous studies showing realistic calculated barriers for several metalloradical reactions of $[Co^{II}(Por)]$ systems.[13] We further incorporated Grimme's dispersion corrections (DFT-D3) for these systems. For the substrate, we included a full model of the azide substrate (4-azidobutyl)benzene. The free energies are depicted in Figure 8 (top). Indeed the transition state barrier (TS_N_2loss) for this step is substantially lower for the $[Co^{II}(Cor)]^-$ system ($\Delta G^{\ddagger}_{298\,K}$ = +14 kcal mol^{-1}) than for the previously reported neutral $[Co^{II}(Por)]$ system ($\Delta G^{\ddagger}_{298\,K}$ = +21 kcal mol^{-1}).[13] Thus, the hypothesis that an anionic electron-rich cobalt(II) corrole complex should be more efficient in the activation of the azide than a corresponding neutral cobalt(II) porphyrin complex indeed holds true. Yet, unfortunately, the temperature needed for this reaction could not be lowered by replacing the neutral $[Co^{II}(Por)]$ complexes by any of the $[Co^{II}(Cor)]^-$ complexes investigated here. We attribute this behaviour to the low solubility of the ionic $[Co^{II}(Cor)]^-$(cobaltocenium$^+$) salts, which immediately precipitate from the toluene solutions upon reduction of the neutral complex at room temperature and are only slowly resolubilised under the catalytic reaction conditions in the presence of azide substrate at 100 °C. Thus, synthesis of $[Co^{II}(Cor)]^-$ complexes with higher solubilities in such low-polarity solvents (benzene or toluene) or replacing the cobaltocenium$^+$ counterions by, for example, tetraalkylammonium cations to increase the solubility may well be a promising strategy to lower the reaction temperatures of the C–H amination reactions in future studies.

We also calculated the spin density of the corrole-based cobalt(III) nitrene complexes. Although the spin density of the parent corrole cobalt(II) complex resides in a different d orbital (d_{xy}) than in the corresponding $[Co^{II}(Por)]$ complex (d_{z^2}), a very similar nitrene radical moiety is formed upon azide activation by the anionic $[Co^{II}(Cor)]^-$ system. As found earlier for the corresponding $[Co^{II}(Por)(N^{\bullet}R)]$ system,[13] the spin density of the $[Co^{II}(Cor)(N^{\bullet}R)]^-$ intermediate is concentrated at the nitrene nitrogen atom (Figure 8, bottom). Thus, it can be expected that the reactions with the anionic $[Co^{II}(Cor)]^-$ complexes are mechanistically related to those proposed previously (Scheme 2), and most likely proceed via very similar cobalt(III)/nitrene radical intermediates, as previously reported for the neutral $[Co^{II}(Por)]$ systems.

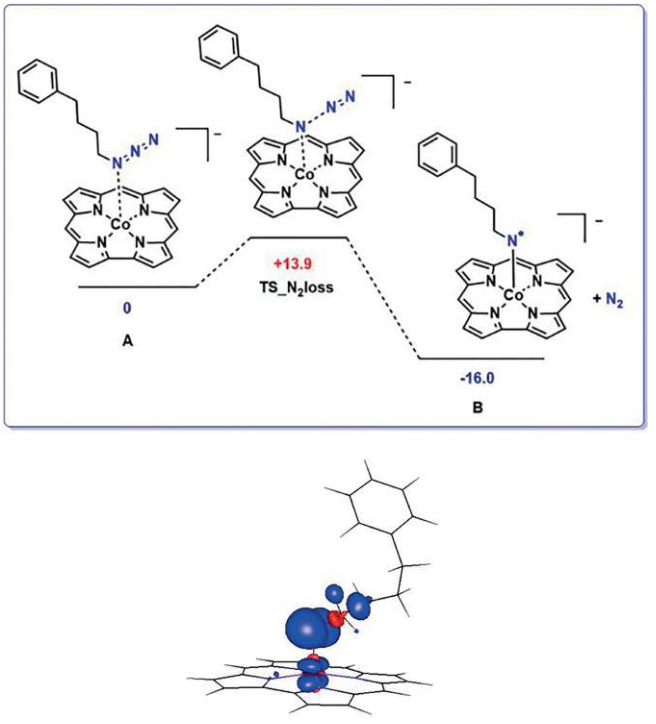

Figure 8. Top: DFT-D3 calculated (Turbomole, BP86, def2-TZVP) free energies $\Delta G^{\circ}_{298\,K}$ [kcal mol^{-1}] for the key step of azide activation by the $[Co^{II}(Cor)]^-$ complex. Bottom: Spin-density plot of nitrene radical intermediate **B**, bearing most of the spin density at the nitrene nitrogen atom.

Conclusions

We have demonstrated that anionic $[Co^{II}(Cor)]^-$ complexes are effective metalloradical catalysts for ring-closing C–H amination of (4-azidobutyl)benzene in the presence of Boc_2O to give the corresponding Boc-protected N-heterocyclic pyrrolidine product (*tert*-butyl 2-phenylpyrrolidine-1-carboxylate). The $[Co^{III}(Cor)(PPh_3)]$ complexes investigated in this study could be chemically reduced to generate the corresponding monoanionic $[Co^{II}(Cor)]^-$ complexes, which are catalytically active in the ring-closing C–H amination reaction of the aliphatic azide. These reduced species were characterised by CV, EPR and UV/Vis spectro-electrochemistry. We demonstrated that the increased electron density of the corrole cobalt(II) complexes compared to porphyrin cobalt(II) complexes increases the rate of the ring-closing C–H amination reaction. Although the reaction temperatures could not be lowered, the reaction times were significantly decreased. In the catalysts tested in this study the reactions were about 2.5 faster than with the corresponding $[Co^{II}(Por)]$ catalysts. However, the selectivity was somewhat compromised. Despite a different starting electronic structure, the thus-produced nitrene species are best described as nitrene-radical intermediates with most of their spin density located at the nitrene nitrogen atom, similar to the nitrene-radical intermediates reported for the neutral $[Co^{II}(Por)]$ systems. In future studies solubility issues will need to be tackled. With more

soluble $[Co^{II}(Cor)]^-$ catalysts in hand, several other metalloradical transformations (carbene- and nitrene-transfer reactions) may become feasible.

Experimental Section

All manipulations were performed under an N_2 atmosphere by using standard Schlenk techniques or in a glove box unless otherwise mentioned. Acetonitrile and CH_2Cl_2 were distilled under nitrogen from CaH_2; THF and toluene were distilled under nitrogen from Na wire. $CoCp_2$ and $CoCp^*_2$ were purchased from commercial sources and stored in the glove box. Mesitylene or trimethoxybenzene was used as internal standard. All ^1H NMR spectra were recorded with a Bruker Avance 400 (400 MHz) or Mercury 300 (300 MHz) spectrometer, referenced internally to the residual protic-solvent resonance of $CDCl_3$ (δ = 7.26 ppm). All $^{13}C\{^1H\}$ NMR spectra were recorded with a Bruker Avance 400 (101 MHz), or Mercury 300 (75 MHz) spectrometer, referenced internally to $CDCl_3$ (δ = 77.2 ppm). High-resolution mass spectra were measured with an AccuTOF LC, JMS-T100LP Mass spectrometer (JEOL, Japan). The FD/FI probe was equipped with FD Emitter, Carbotec or Linden (Germany), FD 10 µm. Current rate 51.2 mA min^{-1} over 1.2 min FI Emitter, Carbotec or Linden (Germany), FI 10 µm. Flashing current 40 mA on every spectrum of 30 ms. Typical measurement conditions: Counter electrode –10 kV, ion source 37 V. (4-Azidobutyl)-benzene was synthesised according to procedure described in literature.[6]

Synthesis of $[Co^{III}(Br_2Cor)(PPh_3)]$: The corrole was synthesised by using the general dipyrromethane condensation method of Gryko and co-workers.[16]

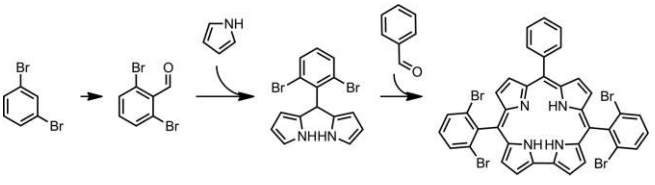

2,6-Dibromphenyl dipyrromethane (1 mmol) and benzaldehyde (0.5 mmol) were dissolved in methanol (100 mL), and H_2O (50 mL) and concentrated (37 %) HCl (5 mL) were added. The mixture was stirred for 2 h. The bilane intermediate was extracted with chloroform and washed with water. The organic layer was dried with Na_2SO_4, filtered and concentrated. The concentrate was diluted to a volume of 250 mL with chloroform, after which *p*-chloranil (1.5 mmol) was added and the mixture allowed to stand overnight without stirring. The mixture was then concentrated and flushed though a plug of silica with dichloromethane. This gave a purple solution, which was concentrated to give 5,15-bis(2,6-dibromophenyl)-10-phenylcorrole as a purple solid. ^1H NMR (400 MHz, $CDCl_3$): δ = 8.99 (d, *J* = 4.2 Hz, 2 H), 8.59 (d, *J* = 4.7 Hz, 2 H), 8.51 (d, *J* = 4.7 Hz, 2 H), 8.40 (d, *J* = 4.2 Hz, 2 H), 8.21–8.16 (m, 2 H), 8.00 (d, *J* = 8.1 Hz, 4 H), 7.72 (dd, *J* = 5.0, 1.7 Hz, 3 H), 7.49 (t, *J* = 8.1 Hz, 2 H) ppm.

5,15-Bis(2,6-dibromophenyl)-10-phenylcorrole (0.1 mmol) was then heated to reflux for 1 h in MeOH (60 mL) together with cobalt acetate tetrahydrate (0.2 mmol) and triphenylphosphane (0.2 mmol). The solution was then concentrated and flushed through a silica plug with dichloromethane as eluent, and the deep red fractions were collected to give the desired cobalt(III) corrole complex. Slow evaporation of a solution in CH_2Cl_2yielded deep red crystals.

^1H NMR (300 MHz, $CDCl_3$): δ = 8.37 (t, *J* = 5.1 Hz, 4 H), 8.27 (d, *J* = 6.5 Hz, 1 H), 8.10 (d, *J* = 4.8 Hz, 2 H), 8.01 (t, *J* = 7.9 Hz, 1 H), 7.80 (dd, *J* = 7.6, 2.7 Hz, 7 H), 7.73 (d, *J* = 4.9 Hz, 3 H), 7.33 (dd, *J* = 16.3, 8.2 Hz, 3 H), 7.00 (t, *J* = 7.5 Hz, 3 H), 6.69 (td, *J* = 7.7, 2.3 Hz, 6 H), 5.17–5.05 (m, 6 H) ppm. ^{13}C NMR (126 MHz, $CDCl_3$): δ = 146.14, 145.61 (d, *J* = 3.3 Hz), 144.39 (d, *J* = 2.3 Hz), 143.28, 142.82, 135.88 (d, *J* = 3.2 Hz), 134.59, 131.00, 130.29, 130.21, 129.24 (d, *J* = 2.7 Hz), 127.58, 127.46–127.27 (m), 127.22, 126.94, 126.58, 126.45 (d, *J* = 2.3 Hz), 125.93, 124.68 (d, *J* = 2.3 Hz), 122.75, 122.09 (d, *J* = 4.5 Hz), 120.74 (d, *J* = 2.6 Hz) ppm. HRMS: calcd. for $C_{55}H_{34}Br_4CoN_4P$ $[M]^+$ 1160.4280, found 1159.7722; calcd. for $C_{37}H_{19}Br_4CoN_4$ $[M - PPh_3]^+$ 898.1362, found 897.7435.

Synthesis of $[Co^{III}(Ph_2Cor)(PPh_3)]$

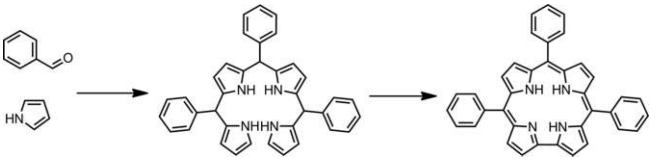

Freshly alumina filtered pyrrole (10 mmol) and benzaldehyde (5 mmol) were dissolved in MeOH (200 mL), and H_2O (200 mL) and concentrated (37 %) HCl (5 mL) were added, after which the reaction mixture was stirred for 3 h at room temperature. The bilane intermediate was extracted with chloroform and washed with water. The organic layer was dried with Na_2SO_4 and filtered. The tetrapyrrole/bilane solution was diluted to a volume of 250 mL of chloroform and kept in the dark from this point on (it is important that these intermediates are handled in the dark). *p*-Chloranil (5 mmol) was added and oxidation of the bilane intermediate was allowed to proceed overnight with stirring. The reaction mixture was concentrated and quickly flushed though a silica plug with dichloromethane. The purity of the solution was checked by TLC (in pure CH_2Cl_2), after which the collected dark green-purple solution was dried to give nearly pure corrole (302 mg, 34 %). In $CDCl_3$ the ^1H NMR spectra was broad, probably due to stacking. The NMR spectrum was therefore recorded in $CDCl_3$ with the addition of a drop of MeOD to prevent stacking. NMR spectra matched those reported in the literature.[25]

The free base 5,10,15-triphenylcorrole (0.3 mmol) was heated to reflux for 1 h in MeOH (180 mL) with cobalt acetate tetrahydrate (0.6 mmol) and triphenylphosphane (0.6 mmol) for 1 h in the dark, after which the solution was concentrated and flushed through a silica plug with dichloromethane as eluent. The deep red fraction containing the desired cobalt(III) corrole complex was collected (91 mg, 36 %).

^1H NMR (300 MHz, $CDCl_3$): δ = 8.60 (d, *J* = 4.4 Hz, 2 H), 8.33 (d, *J* = 4.8 Hz, 2 H), 8.09 (d, *J* = 4.8 Hz, 3 H), 8.03 (d, *J* = 4.6 Hz, 2 H), 7.98 (s, 1 H), 7.68–7.52 (m, 11 H), 7.36 (d, *J* = 7.4 Hz, 1 H), 7.06 (t, *J* = 7.5 Hz, 3 H), 6.76–6.64 (m, 6 H), 4.72 (dd, *J* = 10.7, 8.1 Hz, 6 H) ppm. ^{13}C NMR (126 MHz, $CDCl_3$): δ = 146.27, 145.57, 145.01, 141.88, 136.42, 132.12 (d, *J* = 9.6 Hz), 131.94, 131.74 (d, *J* = 9.2 Hz), 131.55, 130.92, 130.74, 129.85, 129.30, 128.55, 127.63, 127.36, 127.11 (d, *J* = 6.2 Hz), 127.00, 125.39, 124.11, 123.05, 118.58 ppm. HRMS (FD): calcd. for $C_{55}H_{38}CoN_4P$ $[M]^+$ 844.8440, found 844.2140; calcd. for $C_{37}H_{23}CoN_4$ $[M - PPh_3]^+$ 582.5522, found 582.1199.

Synthesis of $[Co^{III}(Mes_2Cor)(PPh_3)]$

The corrole was made by using the hindered dipyrromethane condensation method of Gryko and co-workers.[16] 5-Mesityldipyrromethane (2 mmol) and 2,4,6-trimethoxybenzaldehyde (1 mmol) were dissolved in methanol (200 mL), after which H_2O (100 mL) and

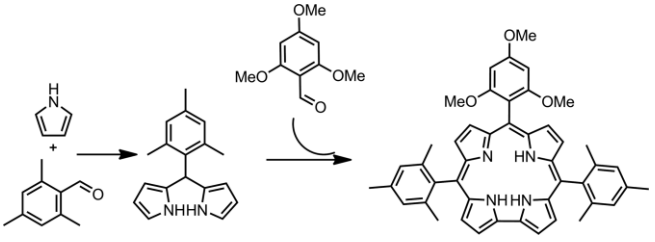

concentrated (37 %) HCl (10 mL) were added. The mixture was stirred for 2 h. The bilane intermediate was extracted with chloroform and washed with water. The organic layer was dried with Na_2SO_4 or $MgSO_4$ and filtered. The tetrapyrrole/bilane solution was from here on kept in the dark, and diluted to a volume of 500 mL with chloroform. *p*-Chloranil (3 mmol) was added in the dark, and oxidation of the bilane intermediate was allowed to proceed overnight with stirring. The mixture was then concentrated and flushed though a silica plug with dichloromethane, and the purple solution was collected to give nearly pure corrole (115 mg, 16 %). The ^{1}H NMR spectra were in accordance with those reported in the literature.[26]

5,15-Dimesityl-10-(2,4,6-trimethoxyphenyl)corrole (0.1 mmol) was heated to reflux for 1 h in MeOH (60 mL) with cobalt acetate tetrahydrate (2 equiv.) and triphenylphosphane (2 equiv.) for 1 h in the dark. After cooling, the solution was condensed and flushed through a silica plug with CH_2Cl_2as eluent, and the deep red fraction containing the CH_2Cl_2 cobalt(III) corrole complex was collected. Crystallization by slow evaporation of a solution in DCM resulted in crystals. The NMR spectrum in pyridine matches that in the literature, which does not show a signal for the PPh_3 ligand.[26]

^{1}H NMR (300 MHz, $CDCl_3$): δ = 8.19 (d, J = 4.6 Hz, 2 H), 8.05 (d, J = 4.4 Hz, 2 H), 7.91 (d, J = 4.7 Hz, 2 H), 7.64 (d, J = 4.4 Hz, 2 H), 7.03 (d, J = 11.4 Hz, 4 H), 6.94 (d, J = 8.0 Hz, 3 H), 6.64 (d, J = 7.9 Hz, 7 H), 6.54 (d, J = 2.2 Hz, 1 H), 6.45 (d, J = 2.2 Hz, 1 H), 5.23 (t, J = 9.4 Hz, 6 H), 4.09 (s, 3 H), 3.66 (s, 3 H), 3.17 (s, 3 H), 2.50 (s, 6 H), 1.74 (s, 6 H) ppm. ^{13}C NMR (126 MHz, $CDCl_3$): δ = 161.55, 159.62, 158.89, 147.52, 145.99, 137.99, 136.77, 136.54, 136.27, 131.68 (d, J = 9.8 Hz), 128.88, 128.12, 127.81, 127.47, 127.19 (d, J = 9.9 Hz), 124.32, 123.00, 122.29, 119.23, 116.01, 114.20, 91.15, 90.89, 56.33, 55.71, 55.40, 29.86, 21.47, 20.42, 19.94 ppm. HRMS (FD): calcd. for $C_{64}H_{56}CoN_4O_3P$ $[M]^+$ 1018.3422, found 1018.3451; calcd. for $C_{46}H_{41}CoN_4O_3$ $[M - PPh_3]^+$ 756.2511, found 756.2512.

Single-Crystal XRD

[$Co^{III}(Br_2Cor)(PPh_3)$]: $C_{55}H_{34}Br_4CoN_4P$ FW = 1160.36, purple-black rough fragment, 0.25 × 0.14 × 0.05 mm, orthorhombic, *Pnma* (no. 62), a = 16.5436(17), b = 19.975(2), c = 13.5943(15) Å, $\alpha = \beta = \gamma$ = 90°, V = 4492.4(8) Å^3, Z = 4, ϱ_{exptl} = 1.716 g cm^{-3}, μ = 4.020 mm^{-1}. In total, 22100 reflections were measured with a Bruker D8 Quest Eco diffractometer, equipped with a TRIUMPH monochromator and a CMOS PHOTON 50 detector (λ = 0.71073 Å) up to a resolution of $(\sin\theta/\lambda)_{max}$ = 0.84 Å^{-1} at a temperature of 150(2) K. The intensity data were integrated with the Bruker APEX2 software.[27] Absorption correction and scaling were performed with SADABS.[28] (0.46–0.75 correction range). In total, 4069 reflections were unique (R_{int} = 0.110), of which 2829 were observed [$I > 2\sigma(I)$]. The structure was solved with direct methods by using the program SHELXS-97[29] and refined with SHELXL-2013 against F^2 of all reflections. Non-hydrogen atoms were refined with anisotropic displacement parameters. Hydrogen atoms were introduced in calculated positions and refined with a riding model. R_1/wR_2 [$I > 2\sigma(I)$]: 0.0581/0.1682. S = 1.025. Residual electron density between –1.174 and 0.677 e Å^{-3}. Geometry calculations and checking for higher symmetry was performed with the PLATON program. The molecular structure is shown in Figure 3.

CCDC 1577156 {for [$Co^{III}(Br_2Cor)(PPh_3)$]} contains the supplementary crystallographic data for this paper. These data can be obtained free of charge from The Cambridge Crystallographic Data Centre.

[$Co^{III}(Mes_2Cor)(PPh_3)$]: The crystal diffracted poorly, but the connectivity between the atoms could be clearly resolved to ascertain the molecular structure shown in Figure 9.

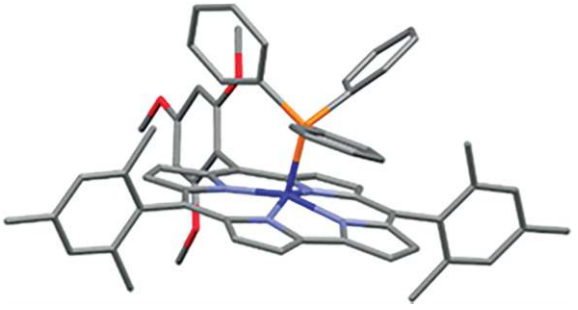

Figure 9. Molecular structure of [$Co^{III}(Mes_2Cor)(PPh_3)$].

CV Measurements: Cyclic voltammograms were recorded with a Metrohm Autolab AUT85221 potentiostat in conjunction with Nova 1.8.17 at a scan rate of 0.1 V s^{-1}. The electrodes used were a glassy-carbon working electrode, a platinum counter electrode and a silver reference electrode. A solution of 0.3 M nBu$_4$NPF$_6$ in dry THF was used as the electrolyte, and potentials were referenced to $Fc^{0/+}$ by using $FeCp_2$* ($E^0_{1/2}$ = –0.45 vs. $Fc^{0/+}$ in THF)[19] as internal reference. These CVs are shown in Figure S1.

Spectro-Electrochemistry: UV/Vis spectro-electrochemistry was performed with an Autolab95 pgstat10 and a Hewlett Packard 8453 spectrometer. Absorbance spectra were recorded with UV/Visible chemstation B.05.02. A solution of 0.3 M nBu$_4$NPF$_6$ in dry THF was used as the electrolyte. The concentration of the corrole complexes was roughly 5×10^{-4} M. The scan speed was 0.02 V s^{-1}. SpectraGryph 1.0.6 was used for processing the spectra. An initial UV/Vis spectrum was recorded before applying any voltage in order to record the spectrum of the neutral compound in THF itself. Following this, the CV was started with further UV/Vis measurements taken every 0.1 V or until the spectrum started to show significant changes, in which case spectra were taken every 0.05 V. This was continued until either –1.0 V was reached or the spectrum no longer showed any changes when the applied potential was increased. For the back-oxidation a similar strategy was followed, by initially taking spectra every 0.1 V until changes in the spectra started to show, after which new spectra were recorded every 0.05 V until 0 V was reached again. These spectra are shown in Figure S2.

EPR Studies: In a glove box, 0.005 mmol of the cobalt corrole complex and 0.75 equiv. of cobaltocene or decamethylcobaltocene {for [$Co^{III}(Mes_2Cor)(PPh_3)$]} were dissolved in dry MeTHF (1.5 mL) and DMSO (0.5 mL), after which 0.2 mL of the resulting solution was transferred to an EPR tube. The spectrum was then measured at 20 K. After the initial measurements, the tubes were opened and the contents exposed to air for ca. 2 min, and then which the tubes were closed and the spectra measured again at 20 K to check for possible effects of minor oxygen leakage. The spectra were recorded on a Bruker EMX-plus spectrometer equipped with a helium cryostat. For additional EPR spectra, see Figure S3.

General Procedure for the Catalytic Reactions: Reactions were performed on 0.3 mmol scale. To a flame-dried and nitrogen-filled Schlenk tube were added catalyst (5 mol-%), (4-azidobutyl)benzene (1 equiv.), Boc_2O (1.1 equiv.) and reductant (5 mol-% cobaltocene) in dry toluene (5.0 mL). The mixture was then stirred for 16 h at 100 °C. After drying, mesitylene or 1,3,5-trimethoxybenzene was added as external standard to determine the yield by NMR spectroscopy (6.1 or 6.8 ppm, respectively). Product peaks at 5–4.75 ppm in $CDCl_3$ were used to determine the yield of the product. NMR-scale reactions were performed using the same method but on 0.06 mmol scale and in [D_8]toluene. Product appearance was monitored by integrating the peaks at 5–4.75 ppm and azide consumption was monitored by means of the decreasing peaks at δ = 3.34 and 2.74 ppm. See Figure S5, for details.

Acknowledgments

We thank Dr. W. I. Dzik (HIMS, UvA) for the X-ray diffraction studies and Ed Zuidinga (HIMS, UvA) for mass measurements. We thank the Netherlands Organization for Scientific Research (NWO-CW VICI grant 016.122.613, BdB) and the University of Amsterdam (RPA Sustainable Chemistry) for financial support.

Keywords: Radicals · Nitrogen heterocycles · Macrocyclic ligands · Cobalt · Amination

[1] R. Hili, A. K. Yudin, *Nat. Chem. Biol.* **2006**, *2*, 284–287.
[2] a) H. M. L. Davies, J. R. Manning, *Nature* **2008**, *451*, 417–424; b) M. P. Doyle, D. C. Forbes, *Chem. Rev.* **1998**, *98*, 911–935; c) H.-J. Lu, X. P. Zhang, *Chem. Soc. Rev.* **2011**, *40*, 1899–1909.
[3] D. Intrieri, P. Zardi, A. Caselli, E. Gallo, *Chem. Commun.* **2014**, *50*, 11440–11453.
[4] a) See ref.[2c]; b) S. Fantauzzi, A. Caselli, E. Gallo, *Dalton Trans.* **2009**, 5434–5443.
[5] a) B. J. Stokes, H. Dong, B. E. Leslie, A. L. Pumphrey, T. G. Driver, *J. Am. Chem. Soc.* **2007**, *129*, 7500–7501; b) C. Jones, Q. Nguyen, T. G. Driver, *Angew. Chem. Int. Ed.* **2014**, *53*, 785–788; *Angew. Chem.* **2014**, *126*, 804; c) Q. Nguyen, T. G. Driver, *J. Am. Chem. Soc.* **2013**, *135*, 620–623; d) D. Intrieri, M. Mariani, A. Caselli, F. Ragaini, E. Gallo, *Chem. Eur. J.* **2012**, *18*, 10487–10490; e) H. Lu, C. Li, H. Jiang, C. L. Lizardi, X. P. Zhang, *Angew. Chem. Int. Ed.* **2014**, *53*, 7028–7032; *Angew. Chem.* **2014**, *126*, 7148.
[6] a) E. T. Hennessy, T. A. Betley, *Science* **2013**, *340*, 591–595; b) E. T. Hennessy, R. Y. Liu, D. A. Iovan, R. A. Duncan, T. A. Betley, *Chem. Sci.* **2014**, *5*, 1526–1532; c) D. A. Iovan, T. A. Betley, *J. Am. Chem. Soc.* **2016**, *138*, 1983–1993; d) N. C. Thacker, Z. Lin, T. Zhang, J. C. Gilhula, C. W. Abney, W. Lin, *J. Am. Chem. Soc.* **2016**, *138*, 3501–3509; e) O. Villanueva, N. M. Weldy, S. B. Blakey, C. E. MacBeth, *Chem. Sci.* **2015**, *6*, 6672–6675; f) D. L. J. Broere, B. de Bruin, J. N. H. Reek, M. Lutz, S. Dechert, J. I. van der Vlugt, *J. Am. Chem. Soc.* **2014**, *136*, 11574–11577; g) D. L. J. Broere, N. P. van Leest, B. de Bruin, B. M. A. Siegler, J. I. van der Vlugt, *Inorg. Chem.* **2016**, *55*, 8603–8611; h) B. Bagh, D. L. J. Broere, V. Sinha, P. F. Kuijpers, N. P. van Leest, B. de Bruin, S. Demeshko, M. A. Siegler, J. I. van der Vlugt, *J. Am. Chem. Soc.* **2017**, *139*, 5117–5124.
[7] a) L.-M. Jin, X. Xu, H. Lu, X. Cui, L. Wojtas, X. P. Zhang, *Angew. Chem. Int. Ed.* **2013**, *52*, 5309–5313; *Angew. Chem.* **2013**, *125*, 5417; b) H. Jiang, K. Lang, H. Lu, L. Wojtas, X. P. Zhang, *Angew. Chem. Int. Ed.* **2016**, *55*, 11604–11608; *Angew. Chem.* **2016**, *128*, 11776; c) V. Subbarayan, L.-M. Jin, X. Cui, X. P. Zhang, *Tetrahedron Lett.* **2015**, *56*, 3431–3434; d) S. Cenini, E. Gallo, A. Penoni, F. Ragaini, S. Tollari, *Chem. Commun.* **2000**, 2265–2266; e) F. Ragaini, A. Penoni, E. Gallo, S. Tollari, C. L. Gotti, M. Lapadula, E. Mangioni, S. Cenini, *Chem. Eur. J.* **2003**, *9*, 249–259.
[8] a) See ref.[7e]; b) H.-J. Lu, V. Subbarayan, J. Tao, X. P. Zhang, *Organometallics* **2010**, *29*, 389–393.
[9] a) J. V. Ruppel, R. M. Kamble, X. P. Zhang, *Org. Lett.* **2007**, *9*, 4889–4892; b) see ref.[5e]; c) H. Lu, J. Tao, J. E. Jones, L. Wojtas, X. P. Zhang, *Org. Lett.* **2010**, *12*, 1248–1251; d) H. Lu, K. Lang, H. Jiang, L. Wojtas, P. Zhang, *Chem. Sci.* **2016**, *7*, 6934–6939; e) H.-L. Jiang, K. Lang, H.-J. Lu, L. Wojtas, X. P. Zhang, *J. Am. Chem. Soc.* **2017**, *139*, 9164–9167; f) H.-J. Lu, H.-L. Jiang, Y. Hu, L. Wojtas, X. P. Zhang, *Org. Lett.* **2012**, *14*, 5158–5161; g) H.-J. Lu, H.-L. Jiang, Y. Hu, L. Wojtas, X. P. Zhang, *Chem. Sci.* **2011**, *2*, 2361–2366.
[10] P. F. Kuijpers, J. I. van der Vlugt, S. Schneider, B. de Bruin, *Chem. Eur. J.* **2017**, asap, https://doi.org/rg/10.1002/chem.201702537.
[11] M. Goswami, V. Lyaskovskyy, S. R. Domingos, W. J. Buma, S. Woutersen, O. Troeppner, I. Ivanović-Burmazović, H. Lu, X. Cui, X. P. Zhang, E. J. Reijerse, S. DeBeer, M. M. van Schooneveld, F. Pfaff, K. Ray, B. de Bruin, *J. Am. Chem. Soc.* **2015**, *137*, 5468–5479.
[12] V. Lyaskovskyy, A. I. O. Suarez, H. Lu, H. Jiang, X. P. Zhang, B. de Bruin, *J. Am. Chem. Soc.* **2011**, *133*, 12264–12273.
[13] P. F. Kuijpers, M. J. Tiekink, W. B. Breukelaar, D. L. J. Broere, N. P. van Leest, J. I. van der Vlugt, J. N. H. Reek, B. de Bruin, *Chem. Eur. J.* **2017**, *23*, 7945–7952.
[14] a) S. Will, J. Lex, E. Vogel, V. A. Adamian, E. Van Caemelbecke, K. M. Kadish, *Inorg. Chem.* **1996**, *35*, 5577–5583; b) K. M. Kadish, J. Shao, Z. Ou, L. Frémond, R. Zhan, F. Burdet, J.-M. Barbe, C. P. Gros, R. Guilard, *Inorg. Chem.* **2005**, *44*, 6744–6754; c) R. Guilard, F. Jérôme, J.-M. Barbe, C. P. Gros, Z. Ou, J. Shao, J. Fischer, R. Weiss, K. M. Kadish, *Inorg. Chem.* **2001**, *40*, 4856–4865; d) K. M. Kadish, Z. Ou, J. Shao, C. P. Gros, J.-M. Barbe, F. Jérôme, F. Bolze, F. Burdet, R. Guilard, *Inorg. Chem.* **2002**, *41*, 3990–4005; e) R. Guilard, F. Burdet, J.-M. Barbe, C. P. Gros, E. Espinosa, J. Shao, Z. Ou, R. Zhan, K. M. Kadish, *Inorg. Chem.* **2005**, *44*, 3972–3983; f) K. M. Kadish, J. Shao, Z. Ou, R. Zhan, F. Burdet, J.-M. Barbe, C. P. Gros, R. Guilard, *Inorg. Chem.* **2005**, *44*, 9023–9038; g) J.-M. Barbe, F. Burdet, E. Espinosa, R. Guilard, *Eur. J. Inorg. Chem.* **2005**, *2005*, 1032–1041; h) J.-M. Barbe, G. Canard, S. Brande's, R. Guilard, *Angew. Chem. Int. Ed.* **2005**, *44*, 3103–3106; *Angew. Chem.* **2005**, *117*, 3163; i) J.-M. Barbe, G. Canard, S. Brande's, R. Guilard, *Chem. Eur. J.* **2007**, *13*, 2118–2129; j) J. M. Barbe, G. Canard, S. Brande's, F. Je'rôme, G. Dubois, R. Guilard, *Dalton Trans.* **2004**, 1208–1214; k) K. M. Kadish, L. Fre'mond, Z. Ou, J. Shao, C. Shi, F. C. Anson, F. Burdet, C. P. Gros, J.-M. Barbe, R. Guilard, *J. Am. Chem. Soc.* **2005**, *127*, 5625–5631; l) B. Mondal, K. Sengupta, A. Rana, A. Mahammed, M. Botoshansky, S. G. Dey, Z. Gross, A. Dey, *Inorg. Chem.* **2013**, *52*, 3381–3387; m) B. Mondal, K. Mittra, A. Mahammed, Z. Gross, A. Dey, *Chem. Commun.* **2017**, *53*, 877–880.
[15] Y. Fang, Z. Ou, K. M. Kadish, *Chem. Rev.* **2017**, *117*, 3377–3419.
[16] B. Koszarna, D. T. Gryko, *J. Org. Chem.* **2006**, *71*, 3707–3717.
[17] P. Madura, W. R. Scheidt, *Inorg. Chem.* **1976**, *15*, 3182–3184.
[18] All redox potentials are reported against the ferrocene/ferrocenium ($Fc^{0/+}$) redox couple. Decamethylferrocene was used as internal standard (E = +0.427 V vs. $Fc^{0/+}$ in THF).
[19] I. Noviandri, K. N. Brown, D. S. Fleming, P. T. Gulyas, P. A. Lay, A. F. Masters, L. Phillips, *J. Phys. Chem. B* **1999**, *103*, 6713–6722.
[20] K. M. Kadish, W. Koh, P. Tagliatesta, D. Sazou, R. Paolesse, S. Licoccia, T. Boschi, *Inorg. Chem.* **1992**, *31*, 2305–2313.
[21] N. G. Connelly, W. E. Geiger, *Chem. Rev.* **1996**, *96*, 877–910.
[22] For similar spectra of reduced [Co^{III}(Cor)] complexes see reference 14m.
[23] In these spectra, contamination by an asymptotic signal was observed, which increased in intensity on exposure to air. This minor signal arises from some small amounts of O_2 leakage, resulting in oxygen binding to the highly reactive reduced species, as reported for related complexes.
[24] a) D. G. H. Hetterscheid, H. Grützmacher, A. J. J. Koekoek, B. de Bruin, *Prog. Inorg. Chem.* **2007**, *55*, 247–253; b) B. A. Goodman, J. B. Raynor, *Adv. Inorg. Chem. Radiochem.* **1970**, *13*, 136–362.
[25] J.-W. Ka, W.-S. Cho, C.-H. Lee, *Tetrahedron Lett.* **2000**, *41*, 8121–8125.
[26] J.-M. Barbe, G. Canard, S. Brandes, F. Jerome, G. Dubois, R. Guilard, *Dalton Trans.* **2004**, 1208–1214.
[27] Bruker, *APEX2 software*, Madison, WI, USA, **2014**.
[28] *SAINT*, version 6.02, and SADABS, version 2.03; Bruker AXS, Inc., Madison, WI, **2002**.
[29] G. M. Sheldrick, *Acta Crystallogr., Sect. A* **2008**, *64*, 112–122.

Received: November 16, 2017